A fluorinated indole-based MDM2 antagonist selectively inhibits the growth of p53[wt] osteosarcoma cells

Lukasz Skalniak[1], **Aleksandra Twarda-Clapa**[1], **Constantinos G. Neochoritis**[2], **Ewa Surmiak**[1], **Monika Machula**[1], **Aneta Wisniewska**[1], **Beata Labuzek**[1], **Ameena M. Ali**[2], **Sylwia Krzanik**[3], **Grzegorz Dubin**[3,4], **Matthew Groves**[2], **Alexander Dömling**[2], and **Tad A. Holak**[1]

[1]Faculty of Chemistry, Jagiellonian University, Gronostajowa 2, 30-387 Krakow, Poland
[2]Department of Drug Design, University of Groningen, Antonius Deusinglaan 1, 9700 AD Groningen, The Netherlands [3]Faculty of Biochemistry, Biophysics and Biotechnology, Jagiellonian University, Gronostajowa 7, 30-387 Krakow, Poland [4]Malopolska Centre of Biotechnology, Jagiellonian University, Gronostajowa 7a, 30-387 Krakow, Poland

Abstract

The p53 protein is engaged in the repair of DNA mutations and elimination of heavily damaged cells, providing anti-cancer protection. Dysregulation of p53 activity is a crucial step in carcinogenesis. This dysregulation is often caused by the overexpression of negative regulators of p53, among which MDM2 is the most prominent one. Antagonizing MDM2 with small molecules restores the activity of p53 in p53 wild-type (p53[wt]) cells and thus provides positive outcomes in the treatment of p53[wt] cancers.

Previously, we have reported the discovery of a panel of fluoro-substituted indole-based antagonists of MDM2. Here, we demonstrate the biological activity and stereoselectivity of the most active compound from this series. Both enantiomers of the esterified form of the compound, as well as its corresponding carboxylic acids, were found active in fluorescence polarization (FP) assay, nuclear magnetic resonance (NMR) and microscale thermophoresis (MST) assay, with K_i and K_D values around 1 μM. From these four compounds, the esterified enantiomer (*R*)-**5a** was

active in cells, which was evidenced by the increase of p53 levels, the induced expression of p53-target genes (*CDKN1A* and *MDM2*), the selective induction of cell cycle arrest and selective growth inhibition of p53^{wt} U-2 OS and SJSA-1 compared to p53^{del} SAOS-2 cells. The analysis of the crystal structure of human MDM2 in complex with the compound (*R*)-**6a** (carboxylic acid of the active (*R*)-**5a** compound) revealed the classical three-finger binding mode. Altogether, our data demonstrate the activity of the compound and provide the structural basis for further structure optimization.

GRAPHICAL ABSTRACT TEXT
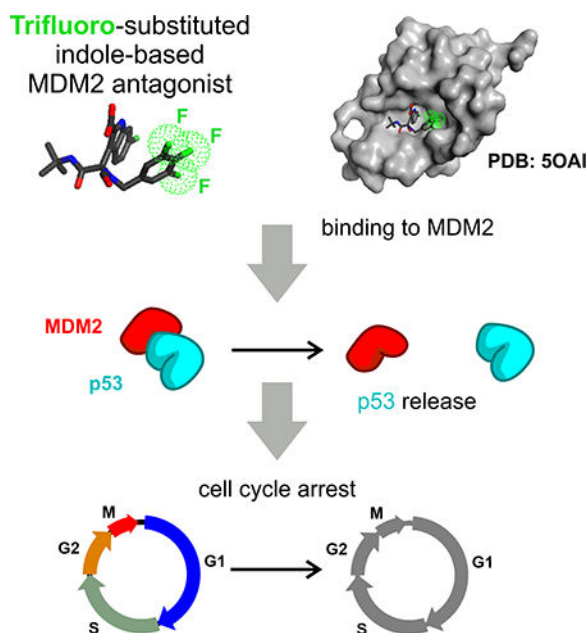
MDM2 antagonists restore the activity of p53 in p53-wild type (wt) cancer cells. Here we demonstrate the biological activity and stereoselectivity of trifluoro-substituted indole-based MDM2 antagonist synthesized by multicomponent Ugi reaction. The compound activates p53, induces cell cycle arrest and selectively inhibits the growth of p53(wt) U-2 OS and SJSA-1 cells compared to p53(del) SAOS-2 cells.

Keywords

p53; MDM2 antagonist; targeted therapy; Ugi reaction; multi-component reaction

INTRODUCTION

The protein p53 is a well-known tumor suppressor, activated in a response to several different stimuli, including DNA damage. Due to its tumor-suppressive activity, p53 is dysregulated in almost every single cancer [1]. It is estimated that 50% of cancers inactivate p53 by gaining loss-of-function mutations or deletions in the *TP53* gene [2]. The remaining 50% of cancers utilize natural mechanisms of negative regulation of p53, enhanced to the extent that disallows its activation. In this regard, the increase of the inhibitory potential of

MDM2 protein is the most common way to keep p53 inactive. MDM2 has the ability to inhibit p53 in the two different ways: by masking the transactivation domain of p53 and by directly ubiquitinating p53, directing the protein to proteasomal degradation [3]. The gene encoding MDM2 protein is very frequently amplified in human cancers, leading to MDM2 overexpression [3]. Overexpressed MDM2 binds to p53, leading to the permanent inactivation of this protein. Accordingly, forced disruption of p53/MDM2 complexes became a favored strategy of the restoration of p53 functioning in p53[wt] cancers [4].

Over the last years, numerous small molecule scaffolds have been proposed, that are able to disrupt the MDM2/p53 complexes. Among these compounds, several presented truly promising preclinical results and are currently undergoing clinical trials [5]. This includes small molecule derivatives of nutlin-3, RG7112 and RG7388 from Roche [6,7], the successor of AM-8553 compound, AMG 232 from Amgen [8], CGM097 and HDM201 from Novartis [9], and spiro-oxindole compounds, SAR405838 (MI-77301) from Sanofi [10], DS-3032b from Daiichi Sankyo [11] and APG-115 from Ascentage Pharma Group [12]. Moreover, several stapled peptides have been described with high affinity toward MDM2 and MDMX, with representative molecule, ALRN-6924 (Aileron Therapeutics), currently undergoing phase I and II clinical trials in patients suffering from solid tumors, lymphoma and myeloid leukemias [5].

In recent years, we have successfully designed and synthesized MDM2 antagonists based on the well-recognized three-point binding model using a pharmacophore-based screening approach and multi-component reaction chemistry [13–21]. Among these reports, we have reported the design, synthesis, and activity of a library of MDM2 antagonists, substituted with fluorine at various positions and synthesized by a classical Ugi four-component reaction (U-4CR) [22]. We showed that the introduction of fluorine substituents to the benzyl group can considerably improve the *in vitro* MDM2 binding activity of the antagonists due to the electrostatic interaction between small molecules and the His96 residue of the protein. We have then identified the most active compound, which was able to the p53/MDM2 interaction with K_i values of 0.13 μM and 0.4 μM for the corresponding acid and ester form, respectively [22]. In the current report, we demonstrate the biological activity of our most potent trifluoro-substituted compound in comparison to known MDM2 antagonists nutlin-3a and Idasanutlin (RG7388). In addition, we report the structural basis of the interaction of our compound (de-esterified) with human MDM2 protein for further structure-based optimization of its properties.

RESULTS

The synthesis of the compounds

Based on our previous work [22], we resynthesized and scaled-up the most promising trifluoro-substituted compound (Figure 1) for further evaluation of its activity employing biochemical, biophysical and cellular assays. The synthesis involves a convergent Ugi 4-component reaction and the MDM2 antagonists can be assembled in just 2 steps from commercially available starting materials [22]. The equimolar mixing of the 3,4,5-trifluorobenzylamine (**1**), the indole-3-carboxaldehyde (**2**), *tert*-butyl isocyanide (**3**) and formic acid (**4**) led to the desired p53-MDM2 antagonist (**5**) (for the detailed description of

synthetic procedures and analytical data see Supporting Information (SI)). The resulting racemic mixture was subjected to preparative chiral separation yielding the two enantiomers, (*R*)-**5a** and (*S*)-**5b** (see the section 1.5 of SI, Figure S1 and Table S1 for the details on the separation of enantiomers). The two latter compounds were hydrolyzed into the corresponding acids (*R*)-**6a** and (*S*)-**6b** (Figure 1).

The compounds 5 and 6 bind to MDM2

Three complementary assays based on independent physicochemical principles, fluorescence polarization (FP), ^{1}H-^{15}N HSQC NMR and microscale thermophoresis (MST) were used to test the *in vitro* activity of the compounds. The FP assay was performed to compare the MDM2-p53 inhibitory activity of new batches of the compounds with the data reported in our previous study [22]. The assay was performed for the enantiomers *R* of the compounds (**5**) and (**6**), as these enantiomers presented higher activity in our previous study [22]. Both compounds presented K_i values much lower than 1 μM, which corresponds well with the values reported previously (see Table 1 and Table S2).

^{1}H-^{15}N HSQC NMR titration was used to verify the results of the FP assay. This method is based on monitoring the chemical shift changes in protein amide backbone resonances upon protein interaction with a small molecule [23–25]. The binding to MDM2 protein was confirmed for all the final compounds, i.e. (*R*)-**5a**, (*S*)-**5b**, (*R*)-**6a** and (*S*)-**6b**. The pattern of chemical shift changes observed for the compound (*R*)-**6a** was similar to the pattern reported in our previous work and also correlates well with the FP data [22]. Tight binding, characterized by the slow chemical exchange and observed as doubling of NMR signals [26] was noted for the compounds (*R*)-**5a**, (*R*)-**6a** and (*S*)-**6b** (Figure 2, Figure S2 and Figure S3). Such a behavior is characteristic for the compounds with dissociation constants K_D values below 1 μM. NMR results showed that acids (*R*)-**6a** and (*S*)-**6b** were more potent compared to their esters (*R*)-**5a** and (*S*)-**5b** (Table 1). This was most evident for the compounds (*S*)-**5b/6b**, for which only acid (*S*)-**6b**, but not the ester (*S*)-**5b**, was able to evoke peaks doubling (Figure S4). For (*S*)-**5b**, though, the spectrum is characteristic for intermediate chemical exchange range which is indicated by broadening and disappearing of peaks like Gly58 or Gly12. For the compounds that undergo intermediate chemical exchange, it is feasible to determine the K_D value [27,28]. The calculated K_D for (*S*)-**5b** was 10.7±6.5 μM (Figure S4). The comparison of enantiomers shows that from the pair of the ester compounds (*R/S*)-**5a/b** the *R*-enantiomer is far more potent than the *S*-enantiomer. In the case of acids (*R/S*)-**6a/b**, both enantiomers exhibit similar potency in the tested system.

Finally, a third assay, microscale thermophoresis (MST) was employed to cross-validate the binding affinity of tested compounds. The technique relies on the thermophoretic motion of the molecule in a temperature gradient induced by a high precision IR-laser beam. Changes in the molecular diffusion resulting from binding events provide information on affinity [29,30].

In the experimental setup, the concentration of a fluorescently labeled MDM2 was fixed at 100 nM, whereas the concentration of an unlabeled binding compound was varied. All the tested compounds showed an affinity towards MDM2 in the low μM range (Table 1, raw

data available in the SI file). The K_D values were 7.0 μM and 1.3 μM for the (*R*)-**6a** and (*S*)-**6b** enantiomers, respectively. Likewise, the binding of ester enantiomers, (*R*)-**5a** and (*S*)-**5b** to the fluorescently labeled MDM2 led to K_D values of 3.0 μM and 7.7 μM, respectively.

The compounds 5 and 6 disrupt the MDM2-p53 complex

As described above, the compounds **5** and **6** bind to MDM2 and are able to displace p53-derived peptide complexed with MDM2 protein. To verify if the compounds are also able to dissociate the p53-MDM2 complex, the compounds were tested by the Antagonist Induced Dissociation Assay (AIDA-NMR) [31].

The method is based on the NMR spectroscopy of the complex formed by the human p53 (residues 1–321) and human MDM2 (residues 1–125), and its subsequent dissociation upon the titration with the inhibitor. Usually the methodology is performed using ^{15}N labeled protein. However, if the distinguished, well separated peaks are observed in ^1H spectra, it is feasible to perform the AIDA-NMR with unlabeled proteins. The analyzed p53-MDM2 complex have the required characteristic signals (around 10 ppm region), originating from the N-terminal p53 domain $^{N}H^e$ indole residues of Trp23, Trp53 and Trp91. Therefore, we decided to perform a proton AIDA-NMR experiments for all the compounds with FP K_i values below 1 μM, and defined as 'tight binders' by the NMR spectroscopy, i.e. the compounds (*R*)-**5a**, (R)-**6a** and (S)-**6b)**, along with a known MDM2 antagonist, nutlin-3a as an reference.

On the 1D proton spectrum of the reference p53-MDM2 complex shows only two peaks, corresponding to Trp91 and Trp53 of p53 (Figure S5). The peak corresponding to the Trp23 is not visible, because this residue is buried inside the protein complex, as it participates in the complex formation. The residues Trp53 and Trp91 are accessible for NMR spectroscopy even when p53 is bound to MDM2 and their corresponding signals are not expected to vary between MDM2-bound and unbound p53. Upon the titration of the complex with MDM2 antagonists, the formation of the peak originating from Trp23 is observed, as exemplified for nutlin-3a (Figure S5 A). This indicates the release of p53 from its complex with MDM2. The p53-MDM2 complex titrated with each of the tested compounds resulted in similar observations, suggesting that the compounds are indeed disrupt p53-MDM2 complex in solution (Figure S5 B-D).

(R)-6a binds to MDM2 with a classical three-finger binding mode

To characterize the structural basis of the interactions of the evaluated compounds at the hydrophobic pocket of the p53-binding domain of MDM2, we determined the crystal structure of (*R*)-**6a** in complex with MDM2(18–125) (fragment of MDM2 comprising residues 18–125). The compound (*R*)-**6a** was chosen as the most potent one in the FP assay. The obtained crystals diffracted to 2.0 Å resolution and contained one protein-inhibitor complex in the asymmetric unit, with (*R*)-**6a** well defined by its electron density (Figure S6) and with no additional inhibitor molecules found within the structure (data collection and refinement statistics shown in the Table S3 in the SI file).

(R)-**6a** binds to MDM2 with a classical three-finger binding mode (Figure 3A,B), occupying all three p53-binding subpockets defined by following residues of p53: Phe19, Trp23, and Leu26 (Figure 3C). Concerning the similarities to the native interaction, the binding of (R)-**6a** into the cleft of MDM2 is primarily stabilized by hydrophobic interactions with Leu54, Leu57, Gly58, Ile61, Met62, Tyr67, Val75, Phe86, Phe91, Val93, Ile99, Tyr100 and Ile103 (residues labeled at Figure 4A). Another resemblance is noticed for the 6-chloroindole substituent of *(R)*-**6a** that inserts into a Trp23 subpocket and assumes an orientation almost identical to the Trp side chain of p53 in the native p53–MDM2 complex. The chlorine atom introduced in *(R)*-**6a** stabilizes the interaction at the bottom of the hydrophobic cleft. Such an arrangement of 6-chloroindole moiety repeating the p53's Trp23 indole interaction follows a canonical binding observed in many different classes of MDM2 inhibitors [32]. Further, comparable to p53 interaction, the NH group within 6-chloroindole participates in a hydrogen bond with the carbonyl oxygen of Leu54 (length of 2.6 Å, Figure 4A).

Concerning the remaining MDM2 subpockets which are naturally occupied by p53's Phe19 and Leu26, the differences can be easily spotted as the character (alkyl/aryl) of substituents of *(R)*-**6a** differs from p53's side chains. The Phe19 subpocket accommodates the *tert*-butyl substituent of *(R)*-**6a** directed at Tyr67. The 3,4,5-trifluorobenzyl substituent of *(R)*-**6a** fills the Leu26 subpocket pointing towards Tyr100 and is involved in π-stacking with His-96 side chain (Figure 4A) [22]. Moreover, this stacking results also in the change of the overall shape of Leu26 subpocket when compared to the native interaction, as in case of *(R)*-**6a** it gets 'closed' and less exposed to the solvent.

Additionally, the inhibitor's scaffold and carboxylic group of *(R)*-**6a** further contribute to the formation of several hydrogen bonds with water molecules interacting with MDM2 (Figure 4B). Taken together, hydrophobic interactions, hydrogen bonds and π-stacking define the high affinity of *(R)*-**6a** to p53-binding pocket of MDM2.

The MDM2 antagonist (R)-5a activates p53 and induces the expression of p53-dependent genes

The disruption of the p53/MDM2 interaction in p53^{wt} cells leads to the release of transcriptionally active p53, which then regulates the expression of a panel of target genes. The protein p21 is a product of such a well-known p53-regulated gene and changes in its expression are often examined to track the activation of p53.

To test the bioactivity of the compounds, human osteosarcoma U-2 OS cells were treated with increasing concentrations of the compounds (R)-**5a** and (R)-**6a** for 24 hours, followed by western blot analysis of the expression of p21 protein. As a control, two MDM2 antagonists were used: Nutlin-3 and RG7388 as one of the best-studied compounds and one of the most potent antagonists, respectively. Both compounds increased the expression of p21 and p53 in U-2 OS cells (Figure 5A). The compound (R)-**5a** induced a strong expression of both p53 and p21 protein, proving the efficient release of p53 from the negative influence of MDM2 (Figure 5A). This effect was observed at the concentrations of

5 and 10 μM of the compound. The carboxylic acid version of (*R*)-**5a**, compound (*R*)-**6a**, did not alter the expression of the examined proteins (Figure 5A).

To check the stereo-selectivity of the compound **5** in living cells, both enantiomers of the compound (**5**), (*R*)-**5a** and (*S*)-**5b**, were tested in a western blot experiment. The analysis confirmed a strong activity of (*R*)-**5a**, while the enantiomer (*S*)-**5b** was found inactive (Figure 5B). This corresponded well with the FP, NMR and MST results, where the enantiomer *S* was found less active than the *R* enantiomer (Table 1).

While the increase of p53 protein levels in response to MDM2 antagonists is due to increased stability of the p53 protein, the increase of expression of p53 targets, p21 and MDM2, is related to transcriptional induction of *CDKN1A* and *MDM2* genes, respectively. To verify if the increased protein levels are associated with increase abundance of corresponding transcript a real-time PCR was performed with the detection of *MDM2*, *CDKN1A* and *TP53* transcripts. The results clearly show that the treatment of U-2 OS cells with MDM2 antagonists, RG7388 or (*R*)-**5a**, leads to a significant increase of *MDM2* and *CDKN1A* transcripts (Figure 5C). This suggest that the (*R*)-**5a** compound indeed indices transcriptional activity of p53 in living cells.

The compound (*R*)-5a selectively inhibits the growth of p53^wt cells

To evaluate the selectivity of (*R*)-**5a** towards p53^{wt} cells, a cell viability MTT assay was performed on two p53^{wt} cell lines, U-2 OS and SJSA-1, and one p53^{del} cell line, namely SAOS-2. Both p53^{wt} cells were more susceptible to (*R*)-**5a** than SAOS-2 cells with the resulting IC$_{50}$ values of 3.3 μM and 2.7 μM for U-2 OS and SJSA-1 cells, respectively, and 13.6 μM for SAOS-2 cells (Figure 5D).

The anticancer activity of MDM2 antagonists results mainly from the induction of cell cycle arrest [33]. To analyze the induction of cell cycle arrest by (*R*)-**5a** flow cytometry analysis was performed. A positive control compound RG7388 decreased the percentage of S-phase cells from 55% to 0.5% in U-2 OS cells at the concentration of 5 μM (Figure 5D). Similarly, (*R*)-**5a** induced cell cycle arrest as demonstrated by the decrease of the percentage of S-phase cells from 55% to 16% and 1.4% at the concentrations of 5 and 10 μM, respectively (Figure 5D). Even stronger cell cycle arrest was observed for SJSA-1 cells, that are known to be extremally sensitive to MDM2 antagonists, but no effect was noted for p53^{del} SAOS-2 cells supporting the activity and selectivity of the compound (Figure S7).

The compound (*R*)-5a induces apoptosis in p53^wt SJSA-1 cells

The activation of p53 with the use of MDM2 antagonists leads not only to the growth inhibition of p53^{wt} cells, but also to the induction of apoptosis, although this effect is restricted to a sub-group of p53^{wt} cells [33–36]. To verify the pro-apoptotic properties of the MDM2 antagonist (*R*)-**5a** a caspase 3/7 activity assay was performed with the use of U-2 OS and SJSA-1 osteosarcoma cells. The cells were treated with staurosporine (positive control), RG7388 (potent MDM2 antagonist), (*R*)-**5a** (active MDM2 antagonist) or (*R*)-**6a** (inactive, de-esterified version of the (*R*)-**5a** compound). Staurosporine induced apoptosis in both cell lines. The active (*R*)-**5a** compound showed the activity similar to RG7388 – it induced

apoptosis only in SJSA-1 cells, and not in U-2 OS cells. Although both cell lines possess wild type p53 protein, SJSA-1 is known to be highly susceptible to apoptosis induced by MDM2 antagonists [33]. Altogether, the results suggest that the compound (*R*)-**5a** presents the bioactivity characteristic for other, well known MDM2 antagonists.

DISCUSSION

In previous studies, we have reported new scaffolds for the design and optimization of MDM2 antagonists, synthesized in one-step multicomponent reactions. We have also performed an exhaustive scanning of fluorine substitutions at the phenyl group of the indole-based compound and provided the proof of the optimized properties of some of the resulting fluoro-substituted compounds. Here, we investigated in detail the strongest MDM2 binder from the previous series. By using three different biophysical techniques we observed strong MDM2 binding of all four final compounds. In accordance with the binding studies, the (*R*)-**5a** enantiomer showed concentration-dependent upregulation of p21 and growth inhibition in different p53 wild-type cell lines. Moreover, the compound showed induction of cell cycle arrest in different wild-type p53 cell lines in low μM concentrations, comparable to the clinical compound RG7388. In contrast, the less-binding (*S*)-**5a** enantiomer was not bioactive *in vitro*. Similarly, the non-esterified compound (*R*)-**6a** had no activity in cells, suggesting that the esterification is necessary for obtaining the biological activity. This may be for example due to increased cell permeability or compound stability.

Currently, several second and third generation MDM2 antagonists are available, with some prominent examples that have entered clinical trials and are evaluated for the treatment of cancer patients [5]. The compound (*R*)-**5a**, presented in this manuscript shows a decent and promising *in vitro* activity, including reactivation of p53 in p53^{wt} cancer cells. However, the structure of the compound would require further development before entering *in vivo* examination, as its activity is revealed at relatively high concentrations (above 1 μM). The crystal structure of (*R*)-**6a**, the de-esterified counterpart of the (*R*)-**5a** compound, bound to MDM2 protein may help in planning of further structure optimization steps. Our recent work suggests that further extending of the compound residue substituents leads to the forced opening of a fourth binding pocket, which, along with the classical Phe19, Trp23, and Leu26 binding pockets, may facilitate the interaction and potentiate the MDM2-antagonizing properties of the compound [13]. For sure the great advantage of the MDM2 antagonist (*R*)-**5a** described in this manuscript lies in its synthesis process, which leads to the generation of a complex chemical entity in a one step, four component Ugi reaction. The structure of the compound (*R*)-**5a** will be further developed in the future to provide better potency and drug-like properties.

MATERIALS AND METHODS

Protein Expression and Purification

Fragments of human MDM2 (residues: 1–118 in pET46; 18–125 - in pET20) were expressed in the *Escherichia coli* BL21-CodonPlus (DE3) RIL strain. Cells were cultured in a total volume of 5 l of LB or minimal medium at 37°C and induced with 1 mM IPTG at OD$_{600nm}$ of 0.8. Protein was expressed for 5 h at 37°C. Cells were collected by

centrifugation (20 min, 5000 g), resuspended in 120 ml PBS with protease inhibitor cocktail and lysed by sonication. Inclusion bodies that were collected by centrifugation (30 min, 18000 g), washed twice with 120 ml PBS containing 0.05% Triton-X100 and once with 120 ml PBS and centrifuged (15 min, 15000 g) after each wash. Purified inclusion bodies were solubilized in 20 ml of 6 M guanidine hydrochloride in 100 mM Tris-HCl, pH 8.0, containing 1 mM EDTA and 10 mM β-mercaptoethanol. The protein was dialyzed against 1 l of 4 M guanidine hydrochloride, pH 3.5 supplemented with 10 mM β-mercaptoethanol. Following, the protein was refolded by dropwise addition into 1 l of 10 mM Tris-HCl, pH 7.0, containing 1 mM EDTA and 10 mM β-mercaptoethanol and slow mixing overnight at 4°C. Ammonium sulfate was added to the final concentration of 1.5 M, mixed for 2 h and centrifuged for 40 min at 10000 g. The refolded protein was recovered on Butyl Sepharose 4 Fast Flow previously equilibrated with refolding buffer containing 1.5 M $(NH_4)_2SO_4$. The column was washed and the protein was eluted using 100 mM Tris-HCl, pH 7.2, containing 5 mM β-mercaptoethanol. Fractions containing the protein were pooled and purified by gel filtration on S75 16/600 column in 5 mM Tris-HCl pH 8.0 containing 50 mM NaCl and 5 mM β-mercaptoethanol (crystallization buffer) or in 50 mM phosphate buffer pH 7.4 containing 150 mM NaCl and 5 mM DTT (FP/NMR buffer).

MDM2-p53 complex expression and purification for the AIDA-NMR

Human MDM2-p53 complex (residues: 1–125 of Mdm2 with poly-histidine tag; 1–321 of p53 in pETDuet-1) were expressed in the *Escherichia coli* BL21-CodonPlus (DE3) RIL strain. Cells were cultured in a total volume of 4 L of LB and induced with 0.5 mM IPTG at OD_{600nm} of 0.7. Protein was expressed for 16 h at 20°C. Cells were collected by centrifugation (20 min, 5000 g), resuspended in 140 ml of 50 mM monosodium phosphate buffer pH 8.0, containing 300 mM sodium chloride and 10 mM imidazole and lysed by sonication. Soluble protein complexes were recovered on Ni-NTA resign previously equilibrated with resuspension buffer. The column was washed with 50 mM monosodium phosphate, pH 8.0, containing 300 mM sodium chloride and 20 mM imidazole and the protein was eluted using 50 mM monosodium phosphate, pH 8.0, including 300 mM sodium chloride and 250 mM imidazole. Fractions containing the complex were pooled and purified by gel filtration on S200 16/60 column in PBS.

Fluorescence Polarization Assay

Fluorescence Polarisation (FP) assay was used to monitor interactions between MDM2 and its antagonists. For each assay, fresh protein stocks of MDM2 (1–118) were thawed and the protein concentrations were determined using the Bradford method. Assay buffer contained 50 mM NaCl, 10 mM Tris pH 8.0, 1 mM EDTA and 5 % DMSO. All the experiments were prepared in duplicates.

The binding affinity of the mutant p53 peptide (P2 peptide, sequence: LTFEHYWAQLTS, labeled with carboxyfluorescein) towards MDM2 was first determined. For this purpose, 10 nM of the fluorescent P2 peptide was contacted with serial dilutions of tested protein (range from 750 to 0.012 nM) in a final volume of 100 μl and fluorescence polarization was determined. K_D was determined by fitting the curve described by below equation to experimental data:

$$FP = FPmin\frac{(\ FPmax - FPmin\ )c}{K_D + c} \quad \text{(I)}$$

where FP is the determined value of fluorescence polarization, FP_{min}- fluorescence polarization for ligand only, FP_{max}- fluorescence polarization at protein concentration saturating the ligand, and c – protein concentration. Competition binding assay was performed using 10 nM fluorescent P2 peptide and optimal protein concentration for the measurement calculated based on determined K_D according to Huang, 2003 ($f_0 = 0.8$) [37]. Tested compounds were dissolved in DMSO at 50 μM. Serial dilutions (50 μM to 0.05 μM) were prepared in DMSO. Nutlin-3a was used as positive controls for MDM2. Fluorescence polarization was determined using Tecan InfinitePro F200 plate reader with the 485 nm excitation and 535 nm emission filters. The fluorescence intensities, parallel and perpendicular to the plane of excitation, were determined in Corning black 96-well NBS assay plates at room temperature. Fluorescence polarization values were expressed in millipolarization units (mP). Inhibition curves were fitted to obtain K_i values.

NMR Experiments

Uniform ^{15}N isotope labeling was achieved by the expression of Mdm2 (residues 1–118) protein in the M9 minimal media containing $^{15}NH_4Cl$ as the sole nitrogen source. The final step of purification of Mdm2 for NMR consisted of gel filtration into the NMR buffer (50 mM phosphate buffer pH 7.4 containing 150 mM NaCl, 5 mM DTT). 10% (v/v) of D_2O was added to the samples to provide lock signal. Water suppression was carried out using the WATERGATE sequence [38]. All the spectra were recorded at 300K using a Bruker Avance 600 MHz spectrometer with Cryo Platform. ^{1}H-^{15}N heteronuclear correlations were obtained using the fast HSQC pulse sequence [39]. Assignment of the amide groups of Mdm2 was obtained after Stoll *et al* [40].

For each compound, the two-dimensional ^{1}H-^{15}N correlated NMR spectrum was recorded at 7–9 different ligand/protein ratios, ranging from 0:1 to 5:1. The samples were prepared by adding small amounts of a 50 mM ligand stock solution in DMSO to the protein solution (0.2 ml) containing the ^{15}N labeled Mdm2 fragment at a concentration of 0.16 – 0.30 mM. The acquisition parameters for each HSQC spectrum was as follows: size of the FID F2: 2048, F1: 100, and a number of scans: 10. Spectra were visualized using *TopSpin 4.0.2*. For the determination of dissociation constants (K_D), nonlinear fits of chemical shifts of single residue versus ligand ratio were performed using the program *OriginPro* (version 9.1) according to the following equation:

$$\Delta_{obs} = \delta_M \frac{\left([P]_0 + [L]_0 + K_D\right) - \sqrt{\left([P]_0 + [L]_0 + K_D\right)^2 - 4[P]_0[L]_0}}{2[P]_0} \quad \text{(II)}$$

Where

$[L]_0$ – ligand concentration

[P]$_0$ – protein concentration

$_{obs}$ – observed chemical shift perturbation normalized according to the Pythagoras formula with ^{15}N weighting factor of 0.2.

δ_M –chemical shift for single residue obtained with maximum ligand concentration

K_D – dissociation constants

The final value of K_D was calculated as a weighted mean value of K_D's obtained for most perturbed residues which undergo fast chemical exchange: Val93, Ile74, and Tyr60.

Microscale Thermophoresis (MST)

Twenty micromolar of the purified human MDM2 protein (residues 1–118) was fluorescently labeled following NanoTemper's Protein Labeling Kit RED-NHS protocol for *N*-hydroxysuccinimide (NHS) (L001- NanoTemper Technologies, Munich, Germany), coupling NT647 dye to lysine residues. The labeled protein was pretested in standard treated, hydrophilic, hydrophobic and premium-coated MST capillaries (NanoTemper Technology) for protein adsorption to the capillary wall; this was evaluated by capillary scans performed by Monolith NT.115 prior to MST experiments.

For MST experiments, the concentration of the labeled MDM2 was kept constant at 100 nM while the unlabeled binding compounds were titrated in 1:1 ratio within 16 two-fold serial dilutions. The compounds stocks were prepared in DMSO (100 mM) and diluted into the assay MST optimized buffer (50 mM Tris-HCl buffer, pH 7.6 containing 150 mM NaCl, 10 mM MgCl$_2$ and 0.05% Tween-20) to reach the final concentration of the assay. Four compounds were tested for binding affinity toward MDM2: **5a,b,** and **6a,b**. Each compound was titrated against a specific amount of MDM2 starting from the highest concentration of 1.25 mM for (*R*)-**6a**, (*S*)-**6b** and (*R*)-**5a** compounds containing 5% DMSO, except (*S*)-**5a** with 0.032 mM as starting highest concentration and 1.5% final DMSO concentration. For the subsequent measurements, serial dilutions were prepared, mixed with MDM2 solution of 200 nM in a final volume of 20 µl and incubated for 4 min. Followed by loading of each reaction mixture into a capillary, placed on the sample tray and then finally transferred to the instrument. MST measurements were taken in Premium-coated capillaries (MO-K025, NanoTemper Technologies) on a Monolith NT.115 instrument using 40% MST power, an LED excitation source with λ = 625n at 22 °C with laser off/on times of 5 s. NanoTemper MO. Affinity Analysis v2.2.4 software was used to fit the data and determine the K_D values.

Protein crystallization

Human MDM2 was prepared in 5 mM Tris pH 8.0, 50 mM NaCl and 5 mM β-mercaptoethanol. Molar excess (3×) of the inhibitor (50 mM stock in DMSO) was added and the MDM2-inhibitor complex was concentrated to 20 mg/ml. Screening for crystallization conditions was performed using a sitting drop vapor diffusion method. Crystals of the MDM2-inhibitor complexes appeared after a few days at 4°C in 0.1 M Bis-Tris pH 6.5 containing 20% (w/v) PEG 5000 MME. MDM2 crystals were flash-cooled in liquid nitrogen without further cryoprotection.

Data collection and crystal structure determination

The diffraction data were collected at 14.1 beamline at the BESSY II, Berlin, Germany. The data was indexed and integrated using XDS [41]. The further computational steps were performed with programs contained in the CCP4 package [42] or Phenix [43]. The data was scaled and merged using Scala [44]. Initial phases for MDM2 structures were obtained by molecular replacement using Phaser [45] and MDM2 structure derived from PDB ID 3TJ2 (MDM2 18–125) as a search model. The models were manually built in the resulting electron density maps using Coot [46]. Restrained refinement was performed using Phenix [43]. After several cycles of model building and refinement, the electron densities defining the ligands in MDM2 structures became clearly visible and the ligand molecule was introduced into the model. The restrains defining the ligand molecule were prepared using JLigand [47]. Water molecules were added using Coot and subsequently manually inspected. The data collection and refinement statistics for all complexes are summarized in Table S2. The structure factors and final models were deposited into PDB with the following accession number: 5OAI.

Cell lines-culture and treatment

Human osteosarcoma cell lines U-2 OS (p53^{wt}) and SAOS-2 (p53^{del}) were purchased from ECACC (Sigma Aldrich) and cultured in McCoy's 5A Medium containing L-glutamine (Lonza) and supplemented with 10% fetal bovine serum (FBS, Biowest). Human osteosarcoma SJSA-1 (p53^{wt}) cell line was purchased from ATCC (LGC Standards) and cultured in RPMI-1640 Medium containing L-glutamine and supplemented with 10% FBS. The cells were cultured at 37°C and 5% CO_2 in a humidified atmosphere and tested for *Mycoplasma* contamination using the PCR-based method [48].

All compounds were prepared as 50 mM stock solutions in DMSO. The compounds were further diluted in DMSO (working solutions, 0.2–20 mM) and added to the culture medium for the cell treatment. The final concentration of DMSO was kept constant and its final concentration was below or equal 0.5%.

Western blot analysis

U-2 OS cells (120 000 cells per well) were seeded on 12-well transparent plates (Falcon). On the next day, the compounds were added and the cells were cultured for an additional 24 h. Cells were lysed with RIPA buffer (Sigma Aldrich) supplemented with protease inhibitor cocktail (Sigma Aldrich). The protein lysates were clarified by centrifugation and analyzed on 12% SDS polyacrylamide gel (Bio-Rad). The proteins were transferred to PVDF membrane (Merck Millipore). The membranes were blocked for 1 h in 4% bovine serum albumin (BSA, Bioshop) in TBS-N buffer (150 mM NaCl, 20 mM Tris-HCl pH 7.6, containing 0.1% Nonidet). Membranes were probed with rabbit monoclonal anti-p21 antibody (1:2000, Cell Signaling, cat. no. 2947) and rabbit monoclonal anti-GAPDH antibody (1:4000, Cell Signaling, cat. no. 2118). Anti-rabbit antibody conjugated with horseradish peroxidase (1:2000, Cell Signaling, cat. no. 7074) was used to detect the primary antibodies. The blots were developed with Clarity Western ECL Substrate (Bio-Rad) and visualized using ChemiDoc MP System (Bio-Rad). Densitometry analysis was performed using ImgeLab software (Bio-Rad).

RNA isolation and real-time PCR

For the isolation of RNA, 120 000 U-2 OS cells were seeded on 12-well plates (Falcon). The next day, the cells were treated for 6 hours with 5 μM RG7388, 10 μM (*R*)-**5a** or DMSO as a control. The total RNA was isolated and purified using PureLink RNA MiniKit (Invitrogen, Thermo Fisher Scientific) supplemented with PureLink DNase (Invitrogen, Thermo Fisher Scientific), according to the manufacturer's protocol. Subsequently, 1 μg of total RNA was used for reverse transcription, performed with the use of M-MLV Reverse Transcriptase (Promega) and oligo-dT primer. After the synthesis, cDNA was amplified in real-time PCR, as described in the manufacturer's protocol, using TaqMan Fast Advanced Master Mix (Thermo Fisher Scientific) with TaqMan Gene Expression Assays for the genes *MDM2* (assay ID: Hs01066930_m1), *TP53* (assay ID: Hs01034249_m1), *CDKN1A* (assay ID: Hs00355782_m1), and *GAPDH* (assay ID: Hs02758991_g1), which was used as a reference gene. The reaction was run on the Eppendorf Realplex 2 System. All samples were run in duplicates. The results were analyzed using the "ΔΔCt" relative quantitation method.

Cell viability MTT assay

U-2 OS cells (500 cells per well), SJSA-1 cells (1000 cells per well) and Saos-2 cells (1000 cells per well) were seeded on 96-well transparent plates (Falcon). Next day the cells were treated with the compounds, prepared at the final concentrations in the fresh culture medium, and cultured for additional 5 days. Thiazolyl blue tetrazolium bromide (MTT, Sigma Aldrich) was added at the final concentration of 0.5 mg/ml and the cells were incubated for 1 h at 37°C. The medium was carefully removed and formazan crystals were dissolved in isopropanol containing 40 mM HCl. The absorbance was measured with Infinite 200 microplate reader (Tecan Group Ltd.) at 570 nm with the reference wavelength 650 nm for background subtraction. Data was analyzed using Origin software (OriginLab). IC_{50} values were calculated by fitting Dose Resp curves to the experimental datasets.

Cell cycle analysis

U-2 OS cells were seeded at 300 000 per 60 15 mm cell culture dish (Eppendorf), treated with tested inhibitors for 24 h, trypsinized and fixed with 70% ethanol. The cell concentration was adjusted to 1×10^6 cells/sample and DNA was labeled with PI-RNase solution (PBS, 5 μg mL-1 propidium iodide, 0.01 mg mL-1 RNase A) for 30 min at 25°C. The cells analyzed for cell cycle DNA content using LSRFortessa cell analyzer (BD Biosciences).

The cells were seeded on cell culture dishes (Eppendorf) and treated next day with DMSO (control), RG7388 or the compounds for additional 24 hours. During the last hour of the treatment, the cells were pulse-labeled with 10 mM bromodeoxyuridine (BrdU, Sigma Aldrich). After that, the cells were harvested by trypsinization and fixed with 96% ethanol in −20 °C for at least 24 hours. Following the fixation, 10^6 cells were centrifuged and the supernatant was removed. Drop by drop, 1 ml of 2N HCl with Triton X-100 (0.5% v/v) was added while vortexing and the cells were incubated at room temperature for 30 min. The cells were centrifuged, supernatant aspirated and the pellet resuspended in 1 ml of 0.1 M $Na_2B_4O_7$, pH 8.5. Following the centrifugation, the supernatant was removed and the cells were resuspended in 0.5 ml of 0.5% Tween/1% BSA/PBS containing 7.5 μl of FITC-

conjugated anti-BrdU antibody (BioLegend, cat. 364104) and stained overnight at 4 °C in the dark with mixing (300 rpm). The cells were centrifuged and the cell pellet was resuspended in 0.5 ml of PBS containing 5 μg/ml of propidium iodide. The cells were analyzed with Fortessa flow cytometer (Becton Dickinson) and BD FACSDIVA software (Becton Dickinson).

Caspase 3/7 activity assay

Caspase 3/7 activity was measured using Caspase-Glo 3/7 Assay (Promega). U-2 OS and SJSA-1 cells were seeded on white 96-wells plates and treated with RG7388, (*R*)-**5a**, (*R*)-**6a** or DMSO for 24 or 48 hours. Staurosporine, a potent inducer of cell apoptosis, was used as a positive control. Next, the plates were equilibrated to room temperature and Caspase-Glo 3/7 Reagent was added directly to the wells. The plates were shaken and kept in the dark at room temperature for 1 h. Luminescence was measured with Infinite 200 microplate reader.

Supplementary Material

Refer to Web version on PubMed Central for supplementary material.

ACKNOWLEDGEMENTS

Abbreviations:

MCR	multicomponent reaction
FP	fluorescence polarization
MDM2	murine double minute-2
MDMX	murine double minute-X
RMSD	root mean square deviation
FBS	fetal bovine serum
DMSO	dimethyl sulfoxide
PVDF	polyvinylidene fluoride
BSA	bovine serum albumin
TBS	Tris-buffered saline

GAPDH	glyceraldehyde-3-phosphate dehydrogenase
MTT	3-(4,5-Dimethylthiazol-2-yl)-2,5-Diphenyltetrazolium Bromide
PBS	phosphate-buffered saline
FITC	fluorescein isothiocyanate
DTT	dithiothreitol
IPTG	isopropyl β-D-1-thiogalactopyranoside
MME	monomethyl ether
PEG	polyethylene glycol
NMR	nuclear magnetic resonance spectroscopy
HSQC	heteronuclear single quantum coherence

REFERENCES

1. Rivlin N, Brosh R, Oren M & Rotter V (2011) Mutations in the p53 Tumor Suppressor Gene: Important Milestones at the Various Steps of Tumorigenesis. Genes Cancer 2, 466–474. [PubMed: 21779514]

2. Soussi T & Wiman KG (2007) Shaping Genetic Alterations in Human Cancer: The p53 Mutation Paradigm. Cancer Cell 12, 303–312. [PubMed: 17936556]

3. Wade M, Li Y-C & Wahl GM (2013) MDM2, MDMX and p53 in oncogenesis and cancer therapy. Nat. Rev. Cancer 13, 83–96. [PubMed: 23303139]

4. Zawacka-Pankau J & Selivanova G (2015) Pharmacological reactivation of p53 as a strategy to treat cancer. *J. Intern. Med.* 277, 248–59. [PubMed: 25495071]

5. Tisato V, Voltan R, Gonelli A, Secchiero P & Zauli G (2017) MDM2/X inhibitors under clinical evaluation: perspectives for the management of hematological malignancies and pediatric cancer. *J. Hematol. Oncol.* 10, 133. [PubMed: 28673313]

6. Tovar C, Graves B, Packman K, Filipovic Z, Higgins B, Xia M, Tardell C, Garrido R, Lee E, Kolinsky K, To K-H, Linn M, Podlaski F, Wovkulich P, Vu B & Vassilev LT (2013) MDM2 small-molecule antagonist RG7112 activates p53 signaling and regresses human tumors in preclinical cancer models. Cancer Res. 73, 2587–2597. [PubMed: 23400593]

7. Ding Q, Zhang Z, Liu J-J, Jiang N, Zhang J, Ross TM, Chu X-J, Bartkovitz D, Podlaski F, Janson C, Tovar C, Filipovic ZM, Higgins B, Glenn K, Packman K, Vassilev LT & Graves B (2013) Discovery of RG7388, a potent and selective p53-MDM2 inhibitor in clinical development. *J. Med. Chem.* 56, 5979–5983. [PubMed: 23808545]

8. Sun D, Li Z, Rew Y, Gribble M, Bartberger MD, Beck HP, Canon J, Chen A, Chen X, Chow D, Deignan J, Duquette J, Eksterowicz J, Fisher B, Fox BM, Fu J, Gonzalez AZ, Gonzalez-Lopez De Turiso F, Houze JB, Huang X, Jiang M, Jin L, Kayser F, Liu JJ, Lo M-C, Long AM, Lucas B, McGee LR, McIntosh J, Mihalic J, Oliner JD, Osgood T, Peterson ML, Roveto P, Saiki AY, Shaffer P, Toteva M, Wang Y, Wang YC, Wortman S, Yakowec P, Yan X, Ye Q, Yu D, Yu M, Zhao X, Zhou J, Zhu J, Olson SH & Medina JC (2014) Discovery of AMG 232, a potent, selective, and orally bioavailable MDM2-p53 inhibitor in clinical development. *J. Med. Chem.* 57, 1454–1472. [PubMed: 24456472]

9. Furet P, Masuya K, Kallen J, Stachyra-Valat T, Ruetz S, Guagnano V, Holzer P, Mah R, Stutz S, Vaupel A, Chène P, Jeay S & Schlapbach A (2016) Discovery of a novel class of highly potent inhibitors of the p53-MDM2 interaction by structure-based design starting from a conformational argument. *Bioorg. Med. Chem. Lett.* 26, 4837–4841. [PubMed: 27542305]

10. Wang S, Sun W, Zhao Y, McEachern D, Meaux I, Barrière C, Stuckey JA, Meagher JL, Bai L, Liu L, Hoffman-Luca CG, Lu J, Shangary S, Yu S, Bernard D, Aguilar A, Dos-Santos O, Besret L, Guerif S, Pannier P, Gorge-Bernat D & Debussche L (2014) SAR405838: an optimized inhibitor of MDM2-p53 interaction that induces complete and durable tumor regression. Cancer Res. 74, 5855–5865. [PubMed: 25145672]

11. Arnhold V, Schmelz K, Proba J, Winkler A, Wünschel J, Toedling J, Deubzer HE, Künkele A, Eggert A, Schulte JH & Hundsdoerfer P (2018) Reactivating TP53 signaling by the novel MDM2 inhibitor DS-3032b as a therapeutic option for high-risk neuroblastoma. Oncotarget 9, 2304–2319. [PubMed: 29416773]

12. Aguilar A, Lu J, Liu L, Du D, Bernard D, McEachern D, Przybranowski S, Li X, Luo R, Wen B, Sun D, Wang H, Wen J, Wang G, Zhai Y, Guo M, Yang D & Wang S (2017) Discovery of 4-((3'R, 4'S,5'R)-6″-Chloro-4'-(3-chloro-2-fluorophenyl)-1'-ethyl-2″-oxodispiro[cyclohexane-1,2'-pyrrolidine-3',3″-indoline]-5'-carboxamido)bicyclo[2.2.2]octane-1-carboxylic Acid (AA-115/APG-115): A Potent and Orally Active Murine Double Minut. *J. Med. Chem.* 60, 2819–2839. [PubMed: 28339198]

13. Bista M, Wolf S, Khoury K, Kowalska K, Huang Y, Wrona E, Arciniega M, Popowicz GM, Holak TA & Dömling A (2013) Transient protein states in designing inhibitors of the MDM2-p53 interaction. Structure 21, 2143–51. [PubMed: 24207125]

14. Neochoritis CG, Wang K, Estrada-Ortiz N, Herdtweck E, Kubica K, Twarda A, Zak KM, Holak TA & Dömling A (2015) 2,30-Bis(10H-indole) heterocycles: New p53/MDM2/MDMX antagonists. *Bioorg. Med. Chem. Lett.* 25, 5661–6. [PubMed: 26584879]

15. Surmiak E, Neochoritis CG, Musielak B, Twarda-Clapa A, Kurpiewska K, Dubin G, Camacho C, Holak TA & Dömling A (2017) Rational design and synthesis of 1,5-disubstituted tetrazoles as potent inhibitors of the MDM2-p53 interaction. *Eur. J. Med. Chem.* 126, 384–407. [PubMed: 27907876]

16. Shaabani S, Neochoritis CG, Twarda-Clapa A, Musielak B, Holak TA & Dömling A (2017) Scaffold hopping via ANCHOR.QUERY: β-lactams as potent p53-MDM2 antagonists†. Medchemcomm 8, 1046–1052. [PubMed: 29034069]

17. Estrada-Ortiz N, Neochoritis CG, Twarda-Clapa A, Musielak B, Holak TA & Dömling A (2017) Artificial Macrocycles as Potent p53-MDM2 Inhibitors. *ACS Med. Chem. Lett.* 8, 1025–1030. [PubMed: 29057045]

18. Guzik K, Zak KM, Grudnik P, Magiera K, Musielak B, Törner R, Skalniak L, Dömling A, Dubin G & Holak TA (2017) Small-Molecule Inhibitors of the Programmed Cell Death-1/Programmed Death-Ligand 1 (PD-1/PD-L1) Interaction via Transiently Induced Protein States and Dimerization of PD-L1. J. Med. Chem 60, 5857–5867. [PubMed: 28613862]

19. Surmiak E, Twarda-Clapa A, Zak KM, Musielak B, Tomala MD, Kubica K, Grudnik P, Madej M, Jablonski M, Potempa J, Kalinowska-Tluscik J, Dömling A, Dubin G & Holak TA (2016) A Unique Mdm2-Binding Mode of the 3-Pyrrolin-2-one- and 2-Furanone-Based Antagonists of the p53-Mdm2 Interaction. *ACS Chem. Biol.* 11, 3310–3318. [PubMed: 27709883]

20. Madhavachary R, Abdelraheem EMM, Rossetti A, Twarda-Clapa A, Musielak B, Kurpiewska K, Kalinowska-Tłu cik J, Holak TA & Dömling A (2017) Two-Step Synthesis of Complex Artificial Macrocyclic Compounds. *Angew. Chem. Int. Ed. Engl.* 56, 10725–10729. [PubMed: 28691783]

21. Koes DR, Dömling A & Camacho CJ (2018) AnchorQuery: Rapid online virtual screening for small-molecule protein-protein interaction inhibitors. Protein Sci. 27, 229–232. [PubMed: 28921842]

22. Huang Y, Wolf S, Koes D, Popowicz GM, Camacho CJ, Holak TA & Dömling A (2012) Exhaustive fluorine scanning toward potent p53-Mdm2 antagonists. ChemMedChem 7, 49–52. [PubMed: 21954050]

23. Powers R (2009) Advances in Nuclear Magnetic Resonance for Drug Discovery. Expert Opin. Drug Discov 4, 1077–1098. [PubMed: 20333269]

24. Shuker SB, Hajduk PJ, Meadows RP & Fesik SW (1996) Discovering high-affinity ligands for proteins: SAR by NMR. Science 274, 1531–4. [PubMed: 8929414]

25. Barile E & Pellecchia M (2014) NMR-based approaches for the identification and optimization of inhibitors of protein-protein interactions. *Chem. Rev.* 114, 4749–63. [PubMed: 24712885]

26. Singh M, Krajewski M, Mikolajka A & Holak TA (2005) Molecular determinants for the complex formation between the retinoblastoma protein and LXCXE sequences. *J. Biol. Chem.* 280, 37868–76. [PubMed: 16118215]

27. Williamson MP (2013) Using chemical shift perturbation to characterise ligand binding. *Prog. Nucl. Magn. Reson. Spectrosc.* 73, 1–16. [PubMed: 23962882]

28. Fielding L (2007) NMR methods for the determination of protein–ligand dissociation constants. *Prog. Nucl. Magn. Reson. Spectrosc.* 51, 219–242.

29. Wienken CJ, Baaske P, Rothbauer U, Braun D & Duhr S (2010) Protein-binding assays in biological liquids using microscale thermophoresis. Nat. Commun 1, 100. [PubMed: 20981028]

30. Jerabek-Willemsen M, Wienken CJ, Braun D, Baaske P & Duhr S (2011) Molecular Interaction Studies Using Microscale Thermophoresis. Assay Drug Dev. Technol 9, 342–353. [PubMed: 21812660]

31. Krajewski M, Rothweiler U, D'Silva L, Majumdar S, Klein C & Holak TA (2007) An NMR-based antagonist induced dissociation assay for targeting the ligand-protein and protein-protein interactions in competition binding experiments. *J. Med. Chem.* 50, 4382–7. [PubMed: 17696513]

32. Popowicz GM, Dömling A & Holak TA (2011) The structure-based design of Mdm2/Mdmx-p53 inhibitors gets serious. *Angew. Chem. Int. Ed. Engl.* 50, 2680–8. [PubMed: 21341346]

33. Skalniak L, Kocik J, Polak J, Skalniak A, Rak M, Wolnicka-Glubisz A & Holak TA (2018) Prolonged Idasanutlin (RG7388) Treatment Leads to the Generation of p53-Mutated Cells. Cancers (Basel). 10, 1–17.

34. Tovar C, Rosinski J, Filipovic Z, Higgins B, Kolinsky K, Hilton H, Zhao X, Vu BT, Qing W, Packman K, Myklebost O, Heimbrook DC & Vassilev LT (2006) Small-molecule MDM2 antagonists reveal aberrant p53 signaling in cancer: implications for therapy. *Proc. Natl. Acad. Sci. U. S. A.* 103, 1888–1893. [PubMed: 16443686]

35. París R, Henry RE, Stephens SJ, McBryde M & Espinosa JM (2008) Multiple p53-independent gene silencing mechanisms define the cellular response to p53 activation. Cell Cycle 7, 2427–2433. [PubMed: 18677110]

36. Huang B, Deo D, Xia M & Vassilev LT (2009) Pharmacologic p53 activation blocks cell cycle progression but fails to induce senescence in epithelial cancer cells. *Mol. Cancer Res.* 7, 1497–1509. [PubMed: 19737973]

37. Huang X (2003) Fluorescence polarization competition assay: the range of resolvable inhibitor potency is limited by the affinity of the fluorescent ligand. *J. Biomol. Screen.* 8, 34–8. [PubMed: 12854996]

38. Piotto M, Saudek V & Sklenár V (1992) Gradient-tailored excitation for single-quantum NMR spectroscopy of aqueous solutions. J. Biomol. NMR 2, 661–5. [PubMed: 1490109]

39. Mori S, Abeygunawardana C, Johnson MO & van Zijl PC (1995) Improved sensitivity of HSQC spectra of exchanging protons at short interscan delays using a new fast HSQC (FHSQC) detection scheme that avoids water saturation. *J. Magn. Reson. B* 108, 94–8. [PubMed: 7627436]

40. Stoll R, Renner C, Hansen S, Palme S, Klein C, Belling A, Zeslawski W, Kamionka M, Rehm T, Mühlhahn P, Schumacher R, Hesse F, Kaluza B, Voelter W, Engh RA & Holak TA (2001) Chalcone derivatives antagonize interactions between the human oncoprotein MDM2 and p53. Biochemistry 40, 336–44. [PubMed: 11148027]

41. Kabsch W (2010) XDS. *Acta Crystallogr. D. Biol. Crystallogr.* 66, 125–32. [PubMed: 20124692]

42. Collaborative Computational Project N 4 (1994) The CCP4 suite: programs for protein crystallography. *Acta Crystallogr.* D. Biol. Crystallogr. 50, 760–3. [PubMed: 15299374]

43. Adams PD, Afonine PV, Bunkóczi G, Chen VB, Davis IW, Echols N, Headd JJ, Hung L-W, Kapral GJ, Grosse-Kunstleve RW, McCoy AJ, Moriarty NW, Oeffner R, Read RJ, Richardson DC, Richardson JS, Terwilliger TC & Zwart PH (2010) PHENIX: a comprehensive Python-based system for macromolecular structure solution. *Acta Crystallogr. D. Biol. Crystallogr.* 66, 213–21. [PubMed: 20124702]

44. Evans P (2006) Scaling and assessment of data quality. *Acta Crystallogr. D. Biol. Crystallogr.* 62, 72–82. [PubMed: 16369096]

45. McCoy AJ, Grosse-Kunstleve RW, Adams PD, Winn MD, Storoni LC & Read RJ (2007) Phaser crystallographic software. *J. Appl. Crystallogr.* 40, 658–674. [PubMed: 19461840]

46. Emsley P, Lohkamp B, Scott WG & Cowtan K (2010) Features and development of Coot. *Acta Crystallogr. D. Biol. Crystallogr.* 66, 486–501. [PubMed: 20383002]

47. Lebedev AA, Young P, Isupov MN, Moroz OV, Vagin AA & Murshudov GN (2012) JLigand: a graphical tool for the CCP4 template-restraint library. Acta Crystallogr. D. Biol. Crystallogr 68, 431–40. [PubMed: 22505263]

48. van Kuppeveld FJ, van der Logt JT, Angulo AF, van Zoest MJ, Quint WG, Niesters HG, Galama JM & Melchers WJ (1992) Genus- and species-specific identification of mycoplasmas by 16S rRNA amplification. *Appl. Environ. Microbiol.* 58, 2606–2615. [PubMed: 1381174]
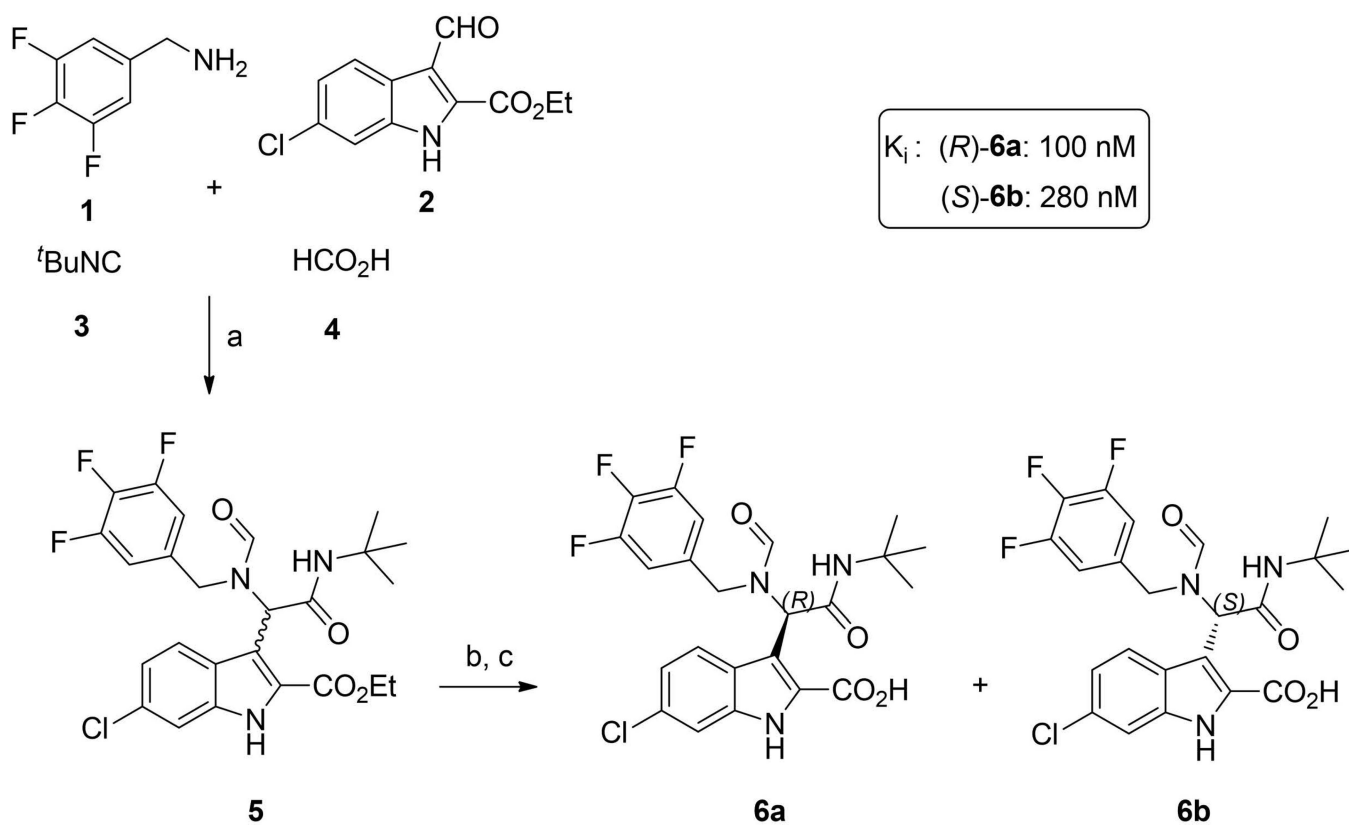
Figure 1. Reactions and conditions for the synthesis of trifluoro-substituted indole-based antagonists.

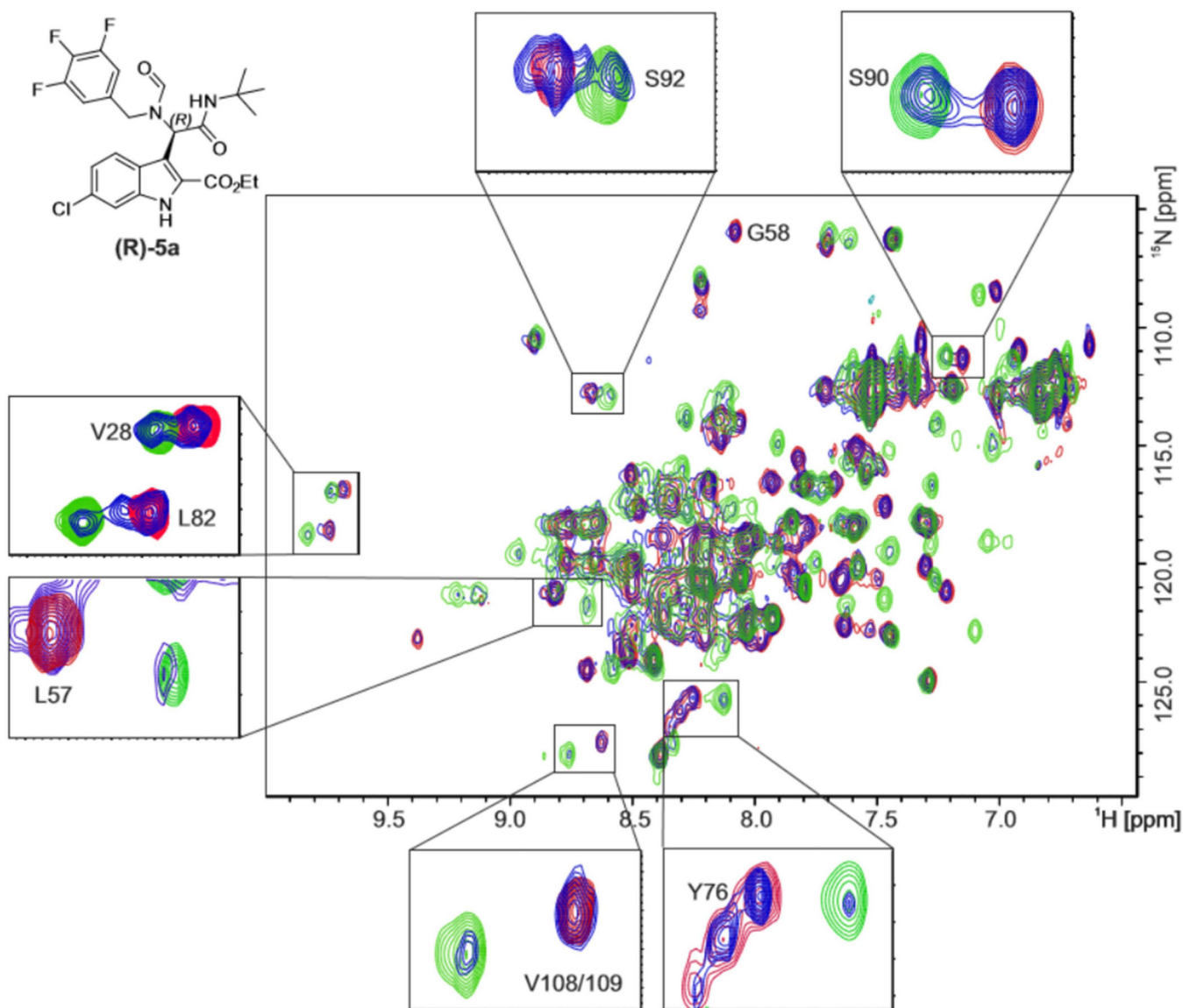(a) rt, MeOH (1.0 M), 2 d, 76% yield; (b) SFC chiral separation; (c) LiOH, EtOH-H_2O, rt, overnight, 95% yield

Figure 2. (*R*)-5a interacts with MDM2 protein.
Titration HSQC-based experiment of the ^{15}N-labeled MDM2 with (*R*)-**5a**: reference MDM2
– red; MDM2:(*R*)-**5a** ratio 3:2 – blue; MDM2:(*R*)-**5a** ratio 5:1 – green; enlarged residues
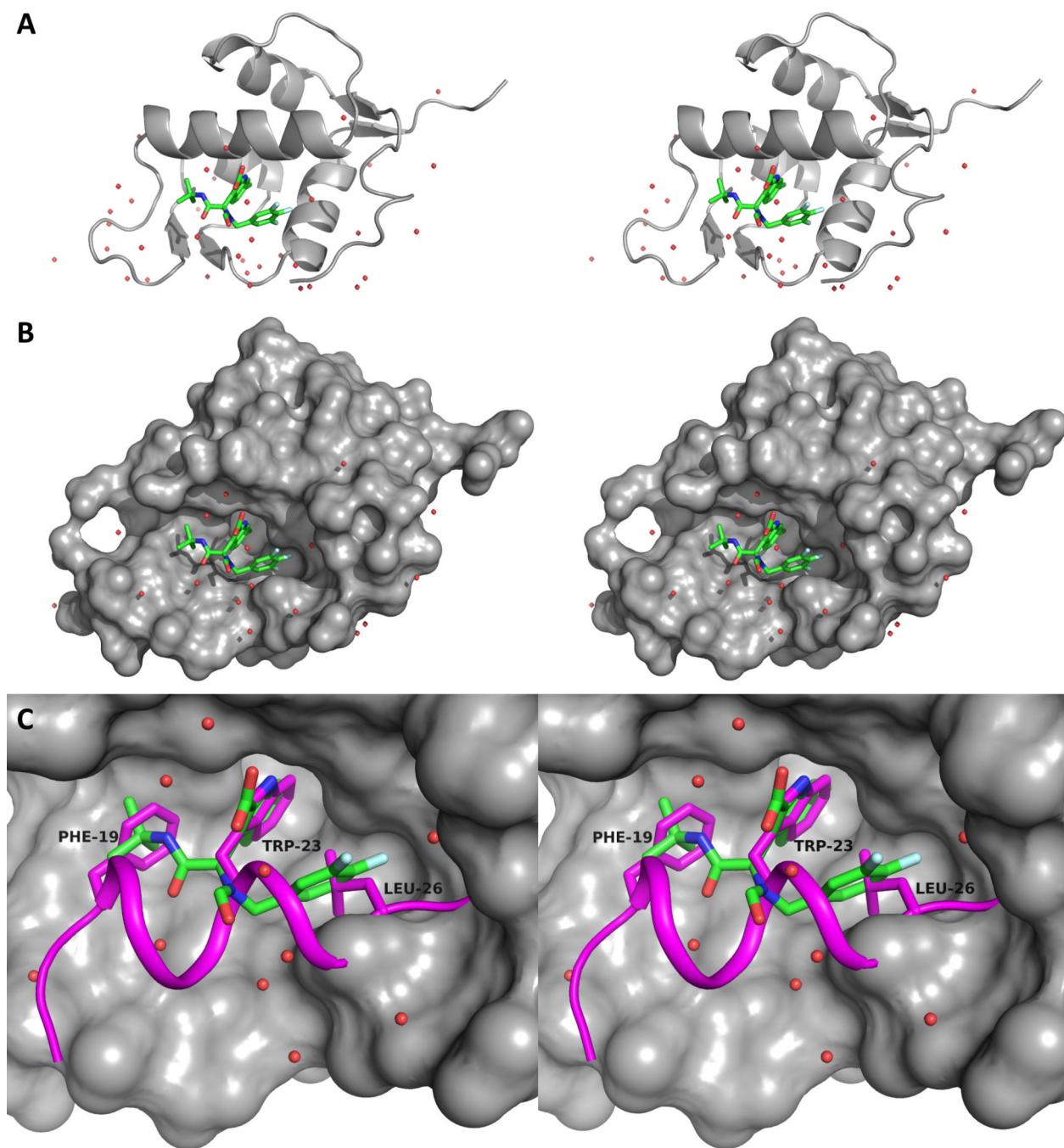that undergoes slow chemical exchange and shows doubling of the peaks.

A

B

C

Figure 3. The binding mode of (*R*)-6a in the hydrophobic pocket of MDM2.
(A,B) Stereoview of (*R*)-**6a** in complex with MDM2 (residues 18–125) – cartoon and surface representation. Inhibitor shown as green sticks, MDM2 shown in grey, waters showed as red spheres; (C) Comparison to p53 peptide, PDB ID 1YCR (shown as magenta ribbon, key residues shown as sticks).
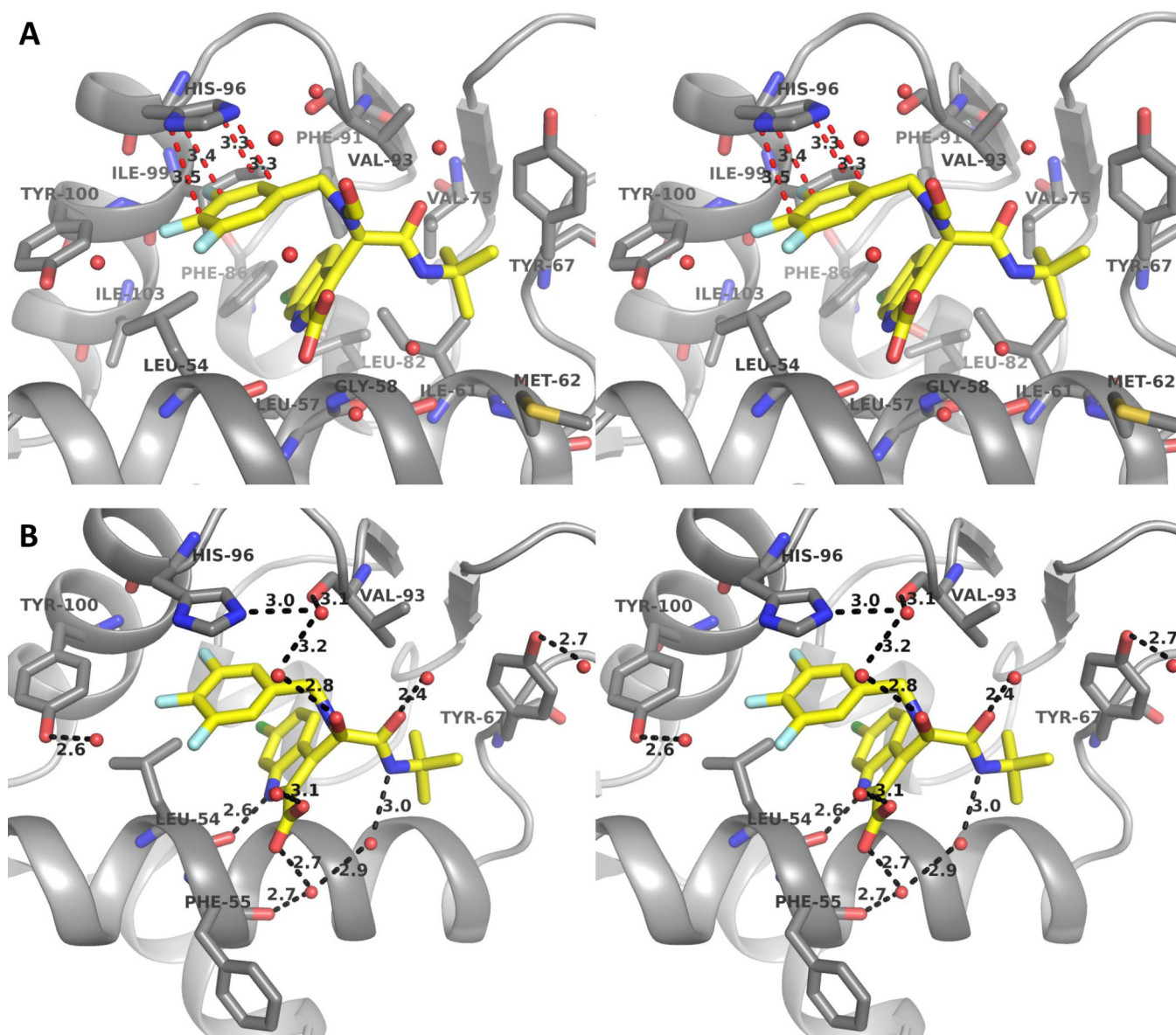
Figure 4. Details of the interaction between (*R*)-6a and MDM2.
(A) Stereoview presenting the π-stacking with His-96 (shown as red dashed lines) and the residues involved in the hydrophobic interactions (shown as grey sticks). Inhibitor shown as yellow sticks, MDM2 shown as grey cartoon; (B) Stereoview presenting the hydrogen bonds (shown as black dashed lines) between (*R*)-**6a** and MDM2/water molecules (shown as red spheres).
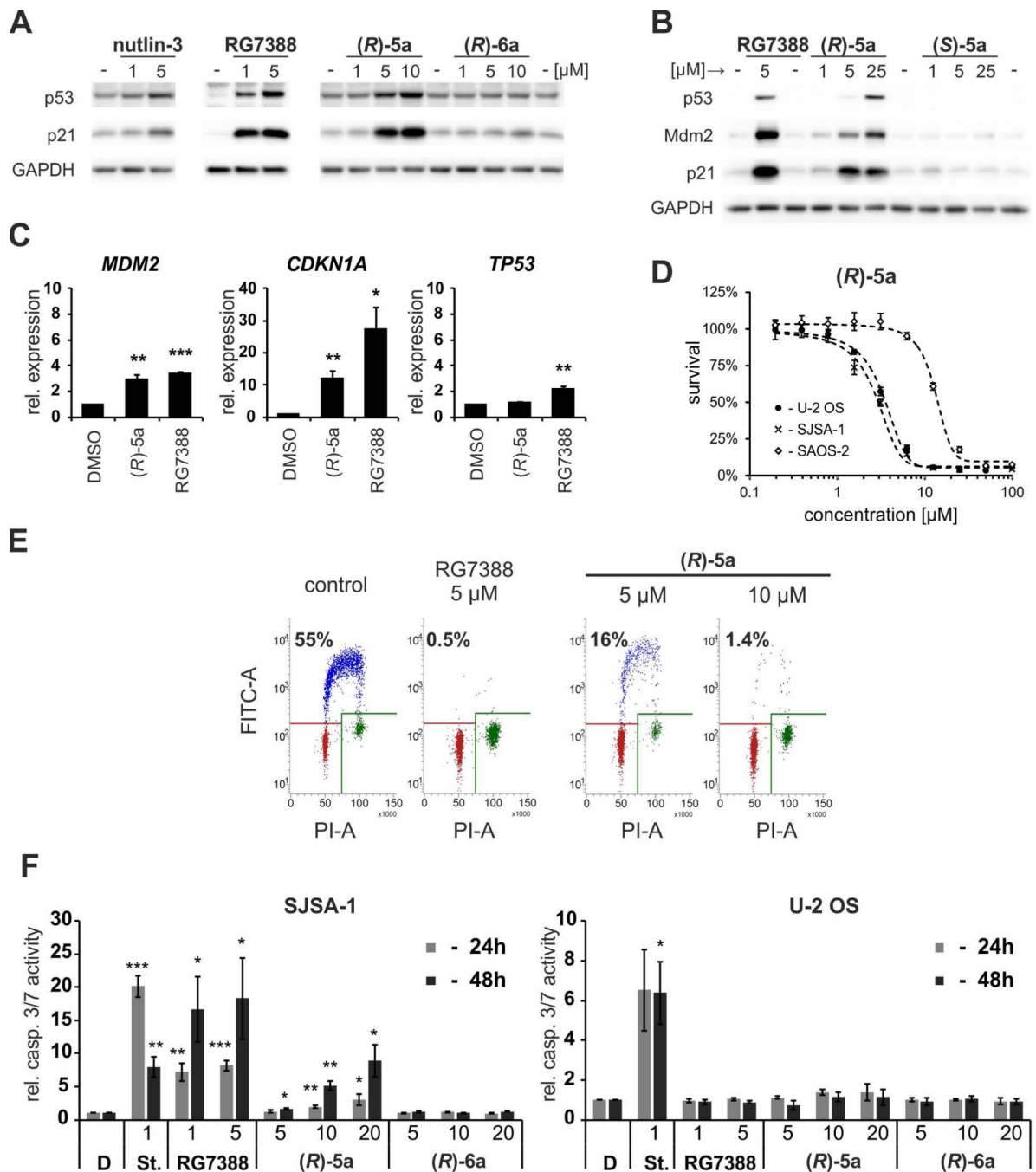
Figure 5. The biological activity of (*R*)-5a, (*S*)-5b, (*R*)-6a and (*S*)-6b compounds.
(A,B) Western blot analysis of the expression of p53, p21 and Mdm2 in U-2 OS cells
following the treatment with the indicated compounds. DMSO-treated cells served as a
control (marked with "**-**"). (C) The expression of p53-target genes (*MDM2* and *CDKN1A*)
and the gene encoding p53 protein (*TP53*). U-2 OS cells were treated with 10 μM of the
compound (*R*)-**5a** or 5 μM RG7388 for 6 hours. DMSO was used as a control. The
expression of genes was quantified by real-time PCR with the use of Taq-Man probes. The
results show mean+SEM values from three experiments, each normalized to *GAPDH*

expression. The statistical significance was evaluated using a *t*-test: * p<0.05, ** p<0.01, *** p<0.001. (D) To test cell viability, MTT assay was performed. U-2 OS (p53^{wt}), SJSA-1 (p53^{wt}) and SAOS-2 (p53^{del}) cells were treated with the indicated concentrations of the tested compounds and cultured for 5 days. The graph shows cell viability normalized to DMSO-treated control cell. (E) Cell cycle analysis of U-2 OS cells treated with the indicated compounds or with DMSO (control). The cells were treated for 24 hours with BrdU pulse-labeling for the last 1 hour of the treatment. The cells were stained with FITC-conjugated anti-BrdU antibody and propidium iodide (PI). The percentages of the cells in the S-phase are given on the plots. (F) Caspase 3/7 activity assay. SJSA-1 and U-2 OS cells were treated with the indicated concentrations of RG7388, (*R*)-**5a**, (*R*)-**6a** or DMSO for 24 or 48 hours. Staurosporine, a potent inducer of cell apoptosis, was used as a positive control. The results show mean+SEM values from three experiments, each normalized to DMSO-treated control cells. The statistical significance was evaluated using a *t*-test versus DMSO-treated control cells: * p<0.05, ** p<0.01, *** p<0.001.

Table 1.

The summary of activities of the trifluoro-substituted compounds. FP – fluorescence polarization assay, NMR - ^{1}H-^{15}N HSQC NMR, MST - microscale thermophoresis.

	cpd. name	FP * K_i [μM]	NMR K_D [μM]	MST K_D [μM]	cell lines	
					activity (p53 induction)	selectivity
esters	(R)-**5a**	0.4	<1	3.0±2.1	**active**	**selective**
	(S)-**5b**	16.7	12.5±3.9	7.7±1.6	not active	not selective
acids	(R)-**6a**	0.1	<1	7.0±2.1	not active	not selective
	(S)-**6b**	0.28	<1	1.3±0.5	not active	not selective

*The given K_i values are retrieved from our previous work [22].